Geochemistry Geophysics Geosystems G3
AN ELECTRONIC JOURNAL OF THE EARTH SCIENCES
Published by AGU and the Geochemical Society

Article
Volume 9, Number 12
23 December 2008
Q12025, doi:10.1029/2008GC002042
ISSN: 1525-2027

Scaling relationships for chemical lid convection with applications to cratonal lithosphere

Norman H. Sleep
Department of Geophysics, Stanford University, Stanford, California 94305, USA (norm@stanford.edu)

A. Mark Jellinek
Department of Earth and Ocean Sciences, University of British Columbia, 6339 Stores Road, Vancouver, British Columbia V6T 1Z4, Canada

[1] We obtain scaling relationships for convection beneath a chemically distinct conducting lid and compare this situation with isochemical stagnant lid convection. In both cases, the vigor of convection depends upon the small temperature contrast across the actively convecting rheological boundary layer, that is, ΔT_{rheo}, the temperature difference between the base of the lid and the underlying half-space. The laterally averaged convective heat flow beneath a chemical lid scales as $q \propto \Delta T_{\mathrm{rheo}}^{4/3}$. Heat flow through a chemical lid approaches a stagnant lid value where the lid does not impact the rheological boundary layer. Such a condition is met when $\Delta T_{\mathrm{rheo}}/T_{\eta} \approx 3.6$, where T_{η} is the temperature change required to change viscosity by a factor of e. We apply our scaling relationships to the slow vertical tectonics of continental interiors: We find that whereas chemical lid convection governs the mantle heat flow to the base of cratons that are underlain by chemically buoyant lithosphere, classical stagnant lid convection governs heat flow into platforms. The laterally averaged heat flow supplied by isochemical stagnant lid convection to platforms has waned as the Earth's mantle cooled. Consequently, the thickness of platform lithosphere, in thermal equilibrium with isochemical stagnant lid convection, has increased over time. Thermal contraction of the thickening platform lithosphere is expected to produce ~300 m subsidence relative to cratons beneath air. This prediction explains why cratons tend to outcrop and platforms tend to be sediment covered.

Components: 9973 words, 17 figures, 2 tables.

Keywords: stagnant lid convection; platform; craton; basin subsidence; lithosphere.

Index Terms: 8103 Tectonophysics: Continental cratons; 8120 Tectonophysics: Dynamics of lithosphere and mantle: general (1213); 8121 Tectonophysics: Dynamics: convection currents, and mantle plumes.

Received 1 April 2008; **Revised** 24 September 2008; **Accepted** 5 November 2008; **Published** 23 December 2008.

Sleep, N. H., and A. M. Jellinek (2008), Scaling relationships for chemical lid convection with applications to cratonal lithosphere, *Geochem. Geophys. Geosyst.*, *9*, Q12025, doi:10.1029/2008GC002042.

1. Introduction and Geological Motivation

[2] Large regions in the interiors of continents are geologically inactive on the time scale of plate tectonics. For purposes of discussion, we loosely divide them into cratons and platforms (Figure 1). Whereas cratonal crust is quite old, typically Archean, >2.5 Ga, platform crust is younger and usually covered by flat lying sediments. Xenolith and diamond inclusion data indicate that these age

Figure 1. Simplified geological map of North America (modified after *Chulick and Mooney* [2002] and *Sleep* [2005]). Dotted line separates platform from the orogens to the east, south and west. Dashed line separates craton from platform. Shallow sediments (tan) cover much of the younger platform crust while much of the Archean crust outcrops. The Michigan and Williston (violet) basins imply several kilometers of platform subsidence.

and chemical differences persists to great depths (i.e., ~200 km) in the lithosphere [e.g., *Griffin et al.*, 2003a, 2003b; *Shirey et al.*, 2003, 2004; *Carlson and Moore*, 2004; *Lehtonen et al.*, 2004]. Both the xenolith studies and geophysical work [*Shapiro et al.*, 1999a, 1999b; *Mooney and Vidale*, 2003] indicate that cratonal lithosphere is chemically buoyant relative to "ordinary" predominately peridotitic upper mantle. We treat platform lithosphere as ordinary mantle on the testable inference that only a thermal boundary layer exists at its base [e.g., *Sleep*, 2005]. The lithosphere beneath cratons is only modestly thicker than the lithosphere beneath platforms [e.g., *Kaminski and Jaupart*, 2000].

[3] We consider the dynamical effects of buoyant cratonal lithosphere in this paper. To put this issue into context, we note that the gravitationally unstable thermal boundary at the base of the lithosphere drives convection in the form of drips beneath both cratons and platforms (Figure 2) [*Jaupart et al.*, 2007]. Without the resulting input of heat from below, the lithosphere would have cooled by conduction down to ~500 km, much greater than the inferred thickness [*Sleep*, 2003a]. We note that viscous dissipation and lateral entrainment of hot material related to drag on the basal boundary layer by plate movements and mantle plumes are insufficient to supply this heat.

[4] Vertical temperature differences across that part of the thermal boundary layer that is involved in convection, the "rheological boundary layer," drive convection (Figure 2) whereas the overlying lithosphere is essentially rigid with a conductive geotherm. Below the boundary layer the mantle is taken to be essentially adiabatic. The convection in the rheological boundary layer can be in one of two regimes, depending on the thickness, buoyancy, and rheology of the chemical layer: (1) Stagnant lid convection results where the strong temperature dependence of mantle viscosity alone causes flow to be confined in a rheological boundary layer. We associate this mode with platforms where the lithosphere has the same composition as the underlying mantle. We denote this situation as "isochemical stagnant lid convection" and use the convectional term "stagnant lid convection" for brevity. (2) "Chemical lid" convection arises where the high viscosity and intrinsic buoyancy of the chemical lid inhibits convection more strongly than the stagnant lid case, resulting in a qualitatively different rheological boundary layer structure. We denote this situation as "viscous chemical lid convection" and expect such behavior beneath cratonal lithosphere. In the special case where the viscosity of the chemical lid is $\geq$100 times the viscosity of the underlying mantle, the lid is effectively rigid and the flow is in a "rigid chemical lid regime."

[5] The problem definition in Figure 2 gives rise to several dynamic questions and potentially to a qualitative understanding of a number of observations related to basic differences between the elevation and structure of platforms and cratons. The current chemical and thermal structure of the lithosphere is inferred from seismology. Xenolith studies constrain the past structure and, in particular, the temperature contrast across the rheological boundary layer and the conductive isotherm. Kimberlites of various ages yield their change over time [*Bell et al.*, 2003; *Sleep*, 2003b].

[6] New scaling relationships for the heat transfer properties of chemical lid convection, compared with established stagnant lid theory, can address the different long-term subsidence histories of platforms and cratons. The adiabatic interior tempera-

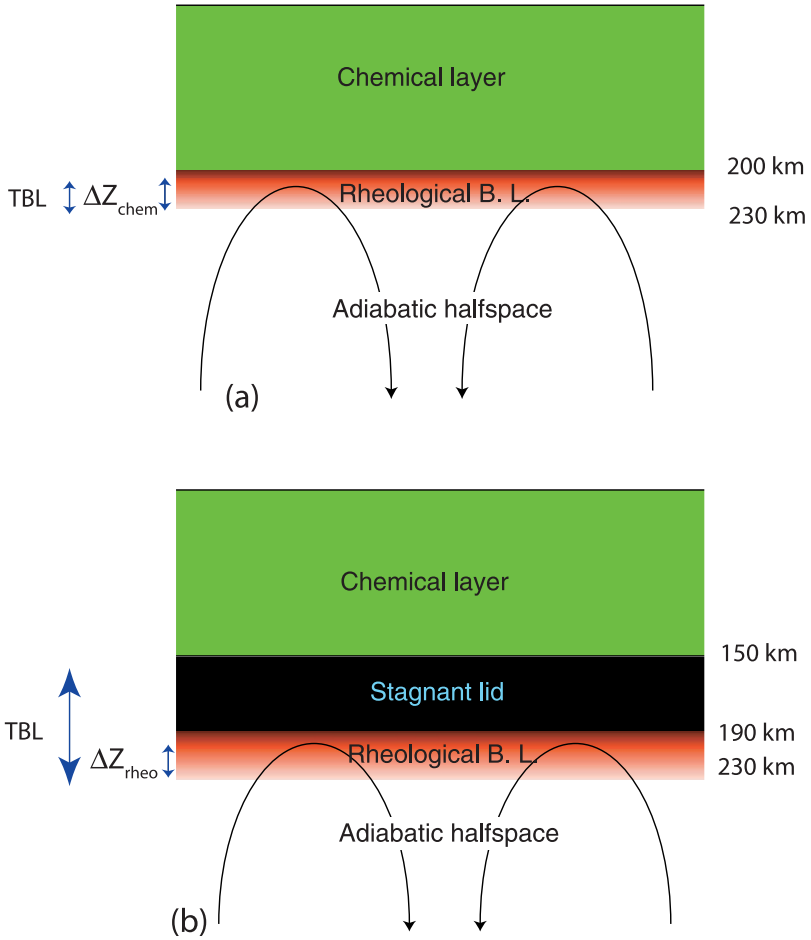

Figure 2. Schematic diagram of (a) chemical lid convection and (b) stagnant lid convection. Temperature contrasts in the rheological boundary layer drive convection. Chemically buoyant material above the stagnant lid has no effect on flow. Approximate depths show where these features are expected beneath cratons. The thermal boundary layer (TBL) is same as the rheological boundary layer for chemical lid convection; it includes both the rheological boundary layer and the stagnant lid for stagnant lid convection.

ture of the Earth's interior has decreased monotonically over the last 3 Ga [*Abbott et al.*, 1994; *Galer and Mezger*, 1998], implying that the laterally averaged heat flow into the base of platform lithosphere has waned. The thickness of platform lithosphere that is in thermal equilibrium stagnant lid convective heat flow has thus increased [*Sleep*, 2005]. The land surface above thickening platform lithosphere subsided from thermal contraction as does the seafloor above thickening oceanic lithosphere. Subsidence on land produces a progressive thickening of the overlying sediment cover, as observed (Figure 1). In contrast, the thickness of chemically buoyant cratonal lithosphere is governed by the thickness of the chemically buoyant lid and thus does not change a priori as the underlying mantle cools.

[7] Eventually the mantle cools enough that the thickness of platform lithosphere in equilibrium with stagnant lid convection becomes thicker than the cratonal chemically buoyant lid. At that time, the chemically buoyant material is too shallow to affect convection. Convection beneath cratons then evolves to the stagnant lid mode and the lithosphere beneath both platforms and cratons cools similarly with time. Cratons on the Earth may be evolving toward this transition at the present time [*Sleep*, 2005].

[8] The purpose of this paper is to obtain scaling relationships relevant to chemical lid convection and its transition to isochemical stagnant lid convection. We appraise and calibrate our results with two-dimensional numerical models. We do limited

laboratory simulations to see how well our dimensional relationships predict heat flow and rheological boundary layer temperature contrast for convection heated from below. We apply the results to the evolution of cratonal and platform lithosphere over geological time.

2. Scaling Relationships

[9] *Lenardic et al.* [2005] and A. M. Jellinek and A. Lenardic (Effects of spatially varying roof cooling on Rayleighh-Bénard convect in a fluid with a strongly temperature-dependent viscosity, submitted to *Journal of Fluid Mechanics*, 2008) address the heat transfer properties of convection beneath a conducting lid in isoviscous and variable-viscosity fluids heated from below and cooled from above. A number of studies suggest, however, that a more appropriate setup for studying convection beneath a craton or platform is transient cooling from above in a fluid with a strongly temperature-dependent viscosity with additional stabilizing buoyancy effects related to chemical layering [e.g., *Cottrell et al.*, 2004; *Jaupart et al.*, 2007]. The major difference from the thermally steady state situation is the absence of rising hot mantle plumes into the base of the lithosphere. *Jaupart et al.* [2007] address the effect of stabilizing chemical buoyancy due to a deformable chemical layer on transient isoviscous thermal convection from a heated boundary. Because of the symmetry of convection in isoviscous systems these authors apply their results to convection beneath a cold craton. This approach is justified because in the stagnant lid limit, commonly assumed to occur beneath the lithosphere, cold drips form in an unstable "rheological boundary layer" that is at most a few times more viscous than underlying mantle. Here, we investigate the heat transfer properties of the complementary and geologically reasonable situation of a rheologically strong "chemical lid" that may or may not extend into the rheological boundary layer, altering the style and heat transfer properties of the flow. We model both stagnant lid convection and chemical lid convection above an adiabatic half-space and investigate transitions between the two regimes.

2.1. Stagnant Lid Scaling

[10] We begin with the well-developed theory of isochemical stagnant lid convection. From the schematic illustration in Figure 2a, chemical lid convection should approach this limit when the approximately rigid chemical layer does not impinge the rheological boundary layer. To maintain generality, we provide a boundary layer derivation with nonlinear viscosity that recovers the scaling relationships from the work of *Solomatov and Moresi* [2000] so we can modify it for the presence of a chemical lid. We ignore depth-dependent viscosity as the derivation is bulky and unrevealing (though straightforward) and as this feature is intractable in the laboratory. With these simplifications, the viscosity is temperature dependent

$$\eta = \eta_0 \exp(\Delta T / T_\eta), \tag{1}$$

where η_0 is the viscosity of the adiabatic half-space, ΔT is the temperature below that in the half-space, and T_η is the temperature scale for viscosity. The quantity T_η is also a scale for the temperature contrast in the boundary layer. Following *Solomatov and Moresi* [2000], we let the rheological temperature contrast be

$$\Delta T_{\text{rheo}} = a_n T_\eta, \tag{2}$$

where a_n is a dimensionless constant of order 1 that depends on n, the power of the rheology. We retain this constant through the derivation with the caveat that (2) still needs to be calibrated experimentally for linear rheology. The thickness of the rheological boundary layer is instantaneously ΔZ_{rheo}. We consider the relevant special case of steady state convection with conduction through the lid. We assume that convection is already finite amplitude so there is no spin-up from a tiny perturbation. The Earth is strongly perturbed by features like passive margins and fracture zones so this is not a problem in practice. One can strongly perturb laboratory and computer models at will.

[11] We constrain the vigor of convection by balancing body forces with viscous forces. The stress from body forces acting on the boundary layer is dimensionally

$$\tau = a_n \rho g \alpha T_\eta \Delta Z_{\text{rheo}}, \tag{3}$$

where ρ is density, g is the acceleration of gravity, and α is the volume thermal expansion coefficient. The strain rate scales with the stress

$$\varepsilon' = \frac{\tau^n}{\tau_{\text{ref}}^{n-1}\eta} = \frac{\tau^n}{\tau_{\text{ref}}^{n-1}\eta_0} \exp(-a_n), \tag{4}$$

where the effective viscosity in the boundary layer is that at the temperature $a_n T_\eta$ below the half-space adiabat. The stress acts on a region that is ΔZ_{rheo} thick so the (vertical) velocity in the boundary

layer is

$$V_V = \varepsilon' \Delta Z_{\text{rheo}} = \frac{\tau^n \Delta Z_{\text{rheo}}}{\tau_{\text{ref}}^{n-1}\eta_0} \exp(-a_n) = \frac{\left(\rho g \alpha a_n T_\eta \Delta Z_{\text{rheo}}\right)^n \Delta Z_{\text{rheo}}}{\tau_{\text{ref}}^{n-1}\eta_0} \exp(-a_n). \quad (5)$$

The convective heat flow is thus,

$$q_v = \rho c V_V a_n T_\eta = \frac{\rho c a_n T_\eta \left(\rho g \alpha a_n T_\eta \Delta Z_{\text{rheo}}\right)^n \Delta Z_{\text{rheo}}}{\tau_{\text{ref}}^{n-1}\eta_0} \exp(-a_n), \quad (6)$$

where ρc is volume specific heat. To this point, we have assumed only that the geotherm is well enough behaved that it is meaningful to define a stagnant lid, a rheological boundary layer, and an underlying adiabatic region.

[12] *Solomatov and Moresi* [2000] make the reasonable assumption that the temperature contrast of the rheological boundary layer self-organizes so the heat flow is a maximum. This occurs when $\partial q_v / \partial a_n = 0$ in (6). This yields

$$a_n \propto (n+1) = 1.2(n+1), \quad (7)$$

where *Solomatov and Moresi* [2000] obtained 1.2 from numerical and laboratory experiments.

[13] Assuming a statistical steady state yields considerable simplification because the thermal gradient in the boundary layer is governed by that in the overlying lithosphere. That is,

$$\frac{\Delta Z_{\text{rheo}}}{Z_L} = \frac{a_n T_\eta}{T_L}. \quad (8)$$

Equating the heat flow through the rigid lithosphere with heat flow into the bottom of the lithosphere gives

$$q = \frac{kT_L}{Z_L} = \frac{\rho c a_n^2 T_\eta^2 \left(\rho g \alpha a_n^2 T_\eta^2 Z_L\right)^n Z_L}{\tau_{\text{ref}}^{n-1}\eta_0 T_L^{n+1}} \exp(-a_n), \quad (9)$$

where k is thermal conductivity. We recover the parameterized stagnant lid result by solving for kT_L/Z_L

$$q_{SL} = kT_\eta \left[\frac{a_n^{2(n+1)} T_\eta^n (\rho g \alpha)^n}{\kappa \tau_{\text{ref}}^{n-1}\eta_0}\right]^{1/(n+2)} \exp(-a_n/(n+2)), \quad (10)$$

where $\kappa \equiv k/\rho c$ is the thermal diffusivity. (Note that one recovers (7) by applying $\partial q_v / \partial a_n = 0$.) For the special case of a Newtonian rheology $n = 1$, (10) simplifies to

$$q_{SL} = ka_1 T_\eta \left[\frac{\rho g a_1 \alpha T_\eta}{\kappa \eta_0}\right]^{1/3} \exp(-a_1/3) = 0.47 kT_\eta \left[\frac{\rho g \alpha T_\eta}{\kappa \eta_0}\right]^{1/3}, \quad (11)$$

where the final calibrated equality comes from the work of *Davaille and Jaupart* [1993a, 1993b, 1994]. We obtain a normalized heat flux or Nusselt number within the boundary layer by dividing the convective heat flow in (6) by the conductive heat flow $q_d = a_n k T_\eta / \Delta Z_{\text{rheo}}$. In this situation, this expression for the Nusselt number is also an effective Rayleigh number for linear viscosity,

$$Ra_{\text{eff}} \equiv \frac{q_v}{q_d} = \frac{\rho g \alpha a_1 T_\eta \Delta Z_{\text{rheo}}^3}{\kappa \eta_0} \exp(-a_1), \quad (12)$$

which provides a measure of the vigor of the flow from the rheological boundary layer (Figure 2). *Solomatov and Moresi* [2000] base their derivations of stagnant lid convection formations on this quantity. For our purposes, it is relevant to modeling time-dependent behavior within the rheological boundary layer.

2.2. Chemical Lid Scalings

[14] The steady state result in (10) and (6) assume that the stagnant lid and the convecting region are composed of one material so that the rheological boundary layer is free to self-organize to its optimal temperature contrast in resulting in the result in (7). This is not true when a rigid conducting lid, like chemically buoyant lithosphere, covers the domain of convection and impinges the rheological boundary layer (Figure 2b). The derivation of (6) and (10) applies, but the rheological boundary exists only below the base of the conducting lid, so that its temperature contrast is $\Delta T_{CL} = AT_\eta$ where A is a dimensionless constant. Like a_1, A refers to the temperature contrast across a rheological layer. The thickness of the rheological boundary layer beneath the lid is $\Delta Z_{\text{chem}} = (A/a_1)\Delta Z_{\text{rheo}}$. In analogy with (11), we find, in turn, a scaling for heat flow through the chemical lid:

$$q_{CL} = kAT_\eta \left[\frac{\rho g A \alpha T_\eta}{\kappa \eta_0}\right]^{1/3} \exp(-A/3). \quad (13)$$

In the Earth, the rheological temperature contrast is much less than the total temperature contrast across the whole lithosphere. Thus, with this picture, the heat flow is approximately that through the

chemical lid with the adiabatic temperature at the base. From (11) and (13) we obtain

$$\frac{q_{CL}}{q_{SL}} = \left[\frac{A}{a_1}\right]^{4/3} \exp[(a_1 - A)/3], \tag{14}$$

or

$$\left[\frac{q_{CL}}{q_{SL}}\right]^{3/4} = \left[\frac{A}{a_1}\right] \exp[(a_1 - A)/4], \tag{15}$$

which applies where the predicted normalized heat flow is between zero and somewhat less than one.

[15] For $(q_{CL}/q_{SL}) \geq 1$, the rheological boundary layer does not impinge on the chemical lid and a stagnant lid limit is recovered. In contrast, as (q_{CL}/q_{SL}) approaches zero, $A \ll a_1$ and $(q_{CL}/q_{SL})^{3/4} \propto A$. In terms of depth, the scale thickness of a lithosphere maintained by stagnant lid convection is

$$Z_{SL} \equiv \frac{kT_L}{q_{SL}} \tag{16}$$

and needs to be greater than the thickness of the chemical lid Z_{chem} in the stagnant lid regime.

[16] To apply (14) and (15), the top of the rheological boundary layer in stagnant lid convection must be defined explicitly, although, temperature, shear tractions, and velocity are continuous. The laterally averaged heat flow asymptotically approaches the conductive gradient and velocities asymptotically approach zero as one moves upward. Traditionally, fluid dynamicists obtain the top from the depth where the difference between the observed thermal gradient and the conductive gradient are not apparent in a laboratory or numerical experiment [*Davaille and Jaupart*, 1993a, 1993b, 1994; *Solomatov and Moresi*, 2000]. This yields $a_1 = 2.4$. By analogy with the stagnant lid (11), we assume that a chemical lid overlying convection (above a given depth) has the same effect on convection as a stagnant lid composed of the isochemical convecting material above that depth. We then obtain this a_1 from numerical experiments.

2.3. Transition Between Stagnant and Chemical Lid Convection

[17] We continue with the case where a chemical lid has a minor effect on convection. As will be discussed in section 5, this situation may prevail beneath cratons on the present Earth. We intend to show how the lid affects convection in that case and to put our scaling relationships into that context. In this case, the normalized temperature contrast between the base of the chemical layer and the adiabatic half-space A is comparable to and mildly greater than the normalized stagnant lid rheological contrast a_1. This formulation is useful because one obtains A in an actual physical or numerical experiment by measuring laterally averaged temperature at the base of the chemical lid. In this limit, chemically buoyant material does not circulate and contribute to the convective heat flow.

[18] We illustrate the case using our previous derivation. Heat flow and velocity ratios provide a convenient and useful way to define a transition from a stagnant lid to chemical lid regime and also to characterize the nature of this transition.

[19] We make the assumption that the chemical lid is rigid in this section to simplify calculations. The corresponding stagnant lid is very viscous at the depths where the chemical lid is present (i.e., the strain rate $\varepsilon' > 0$, although this part of the cold boundary layer does not take much part in the flow). The laterally averaged thermal gradient is thus essentially the conductive gradient in both regions (Figure 3). We define a vertical coordinate z above the depth where the conductive geotherm extrapolates to the mantle abiabat. The temperature deficit relative to the mantle adiabat is then

$$\Delta T = \frac{zT_L}{Z_L} \tag{17}$$

The convective heat flow is the product of this temperature contrast and the velocity. We obtain the velocity with an integral of strain rate from a fixed point in the rigid part of the lid. The integral in the stagnant lid is

$$V_{SL} = -\int_{\infty}^{z} \frac{\tau}{\eta_0} \exp\left[\frac{-\Delta T}{T_\eta}\right] dZ = -\int_{\infty}^{z} \frac{\tau}{\eta_0} \exp\left[\frac{-T_L Z}{Z_L T_\eta}\right] dZ, \tag{18}$$

where Z is the dummy variable for z and the lower limit of the rapidly convergent integral (representing the physical upward rigid lithosphere) is taken to infinity. The corresponding chemical lid velocity is

$$V_{CL} = -\int_{Z_{CL}}^{z} \frac{\tau}{\eta_0} \exp\left[\frac{-\Delta T}{T_\eta}\right] dZ = -\int_{Z_{CL}}^{z} \frac{\tau}{\eta_0} \exp\left[\frac{-T_L Z}{Z_L T_\eta}\right] dZ, \tag{19}$$

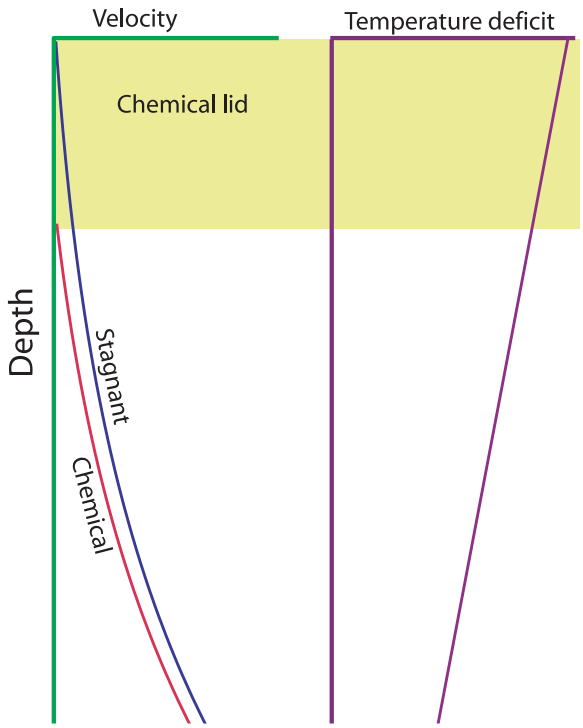

Figure 3. The convective heat flow is the integral of (left) the product of the convective velocity and (right) the temperature deficit relative to the mantle adiabat. The velocity within the chemical lid is zero and less than the velocity within the stagnant lid below the chemical lid.

where Z_{CL} is the distance of the base of the chemical lid above the depth where the geotherm extrapolates to the mantle adiabat. The chemical lid has two effects on heat flow (Figure 3). There is a direct effect in that the velocity in the chemical lid is zero. There is an indirect effect that the velocity beneath the chemical lid is everywhere slightly lower than the stagnant lid velocity. For example, the velocity difference at the base of the chemical lid is

$$V_{SL} - V_{CL} = -\int_{\infty}^{Z_{CL}} \frac{\tau}{\eta_0} \exp\left[\frac{-T_L Z}{Z_L T_\eta}\right] dZ = \frac{\tau Z_L T_\eta}{\eta_0 T_L} \exp\left[\frac{-T_L Z_{CL}}{Z_L T_\eta}\right], \quad (20)$$

where the final equality includes our previous assumption that that the stress in (3) is independent of depth in the nearly rigid part of the stagnant lid. The term within the final exponential is $-A$. That is, the velocity difference and the heat flow difference approach zero as the temperature contrast between the base of the chemical lid and the mantle adiabat increases.

[20] We conclude the derivation at this point, as the dimensional integrals of the convective heat flow difference $\rho C(V_{Sl} - V_{CL})\ \Delta T$ are straightforward but not revealing. A more precise formulation would require modifying (17) so that it represents the thermal gradient within the lower hotter part of the boundary layer. We note that the formulism in section 5 for continental freeboard provides a convenient analytical expression for the geotherm for this task.

3. Numerical Models

[21] We compute two-dimensional thermal models to calibrate our scaling relationships using the stream function code by *Sleep* [2002, 2003a, 2003b, 2005, 2006, 2007]. We impose a rigid conducting lid from 197.5-km depth to the surface where it was 0°C. The models have a 5-km grid. We use the thermal gradient to show that this grid spacing is sufficiently dense to resolve viscosity changes. The steepest thermal gradient occurs at the top of the thermal boundary layer (and within the overlying lithosphere). The gradient at the base of ~200 km thick lithosphere is ~6 K km^{-1}, implying a 30 K change across a grid in the models. We use T_η = 60 and 100 K in our models. Thus viscosity changes by a factor of at most 1.65 and 1.35, respectively, across a grid.

[22] We define temperature at integers times 5-km points in depth and horizontal coordinate. We define the stream function at integer times 5-km plus 2.5-km points. This boundary condition naturally applies at stream function nodes. We apply no-slip boundary conditions where both the horizontal and vertical velocities are zero at the boundary to represent the laboratory case where the conducting lid has the same conductivity as the convecting fluid. We compute four models with a chemically buoyant layer that extends initially from the surface to 197.5-km depth with the free-slip condition at the Earth's surface. As we define composition nodes at integral times 5-km nodes, the implied interface is halfway between the chemical lithosphere nodes at 195-km depth and the ordinary mantle points at 200-km depth.

[23] The domain of the calculation is 900-km wide, giving an aspect ratio of ~4 within the sublithospheric region that convects. We apply free-slip mechanical boundary conditions at each end and no horizontal heat flow as a thermal boundary condition. We apply a permeable bottom boundary condition at 500-km depth to represent a large

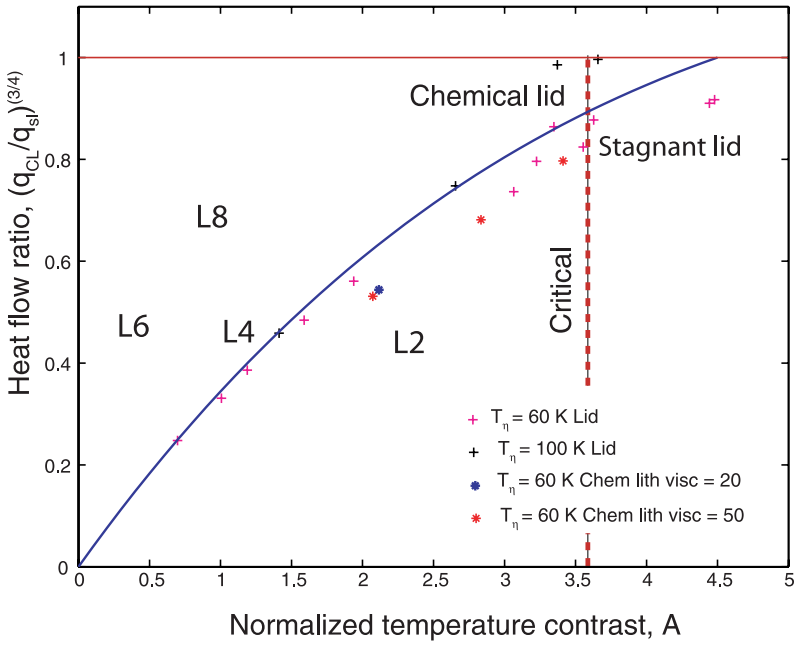

Figure 4. Numerical and laboratory results appraise the scaling relationship (14) for a rigid chemical lid. The rigid chemical lid models for $T_\eta = 60$ K and $T_\eta = 100$ K and the viscous chemical lid models where the lithosphere is a factor or 20 or 50 more viscous than normal mantle plot together, indicating that the relationship applies to the first order. The eyeball curve (21) provides a good fit extrapolating linearly to the origin for small values of the rheological temperature contrast but the numerical points scatter as the stagnant lid limit is approached. The laboratory experiment heated from below with a continuous rigid lid has a dimensionless temperature contrast of 5.54 and does not plot on the graph. Points L are laboratory experiments heated from below with a partial chemical lid. The coverage of the lid is 20%, 43%, 60%, and 83% for points L2, L4, L6, and L8, respectively. They do not line along the trend of the numerical experiments indicating that the scaling relationship does not adequately represent this situation. We show the critical value of $A = 3.6$ for transition to stagnant lid behavior obtained below from additional models.

underlying adiabatic region. Fluid enters the domain at the potential temperature of 1300°C. There is constant pressure at the boundary so that it does no work on the domain of the model. There is also no horizontal velocity at the boundary.

[24] We do not vary well-constrained parameters in our generic models. These include the thermal expansion coefficient $\alpha = 3 \times 10^{-5}$ K^{-1}, volume specific heat $\rho C = 4 \times 10^6$ J m^{-3} K^{-1}, thermal conductivity $k = 3$ W m^{-1} K^{-1}, the potential temperature of the mantle adiabat $T_L = 1300$°C, the density $\rho = 3400$ kg m^{-3}, and the acceleration of gravity 9.8 m s^{-2}. We compute only models with linear (Newtonian) viscosity ($n = 1$) for simplicity.

3.1. Chemical Lid Models

[25] We begin with models where the rigid chemical lid has a major effect on the flow (Figure 4). We plot the laterally averaged heat flow and the laterally averaged temperature contrast between the boundary and the adiabat, A in normalized notation. We allow the models to approach steady state values of these parameters.

[26] The linear scaling suggested by (15) works for modest values of $A \leq 2$. Models with $T_\eta = 60$ K plot together with models with $T_\eta = 100$ K. We also plot normalized points that explicitly represent the chemically buoyant lithosphere. Models with the viscous chemical layer a factor of 20 or 50 more viscous than ordinary mantle plot with the rigid chemical lid results. This indicates that the no-slip, conducting lid is a reasonable representation of a viscous chemical lid, like cratonal lithosphere. We plot a curve with the form of (15) and obtain an approximate fit to the data with:

$$\left[\frac{q_{CL}}{q_{SL}}\right]^{3/4} = \left[\frac{A}{4.5}\right] \exp[(4.5 - A)/8]. \qquad (21)$$

Model 1 illustrates the behavior well into the rigid chemical lid regime (Figure 5). The viscosity is 0.2×10^{18} Pa s and $T_\eta = 60$ K. These parameters

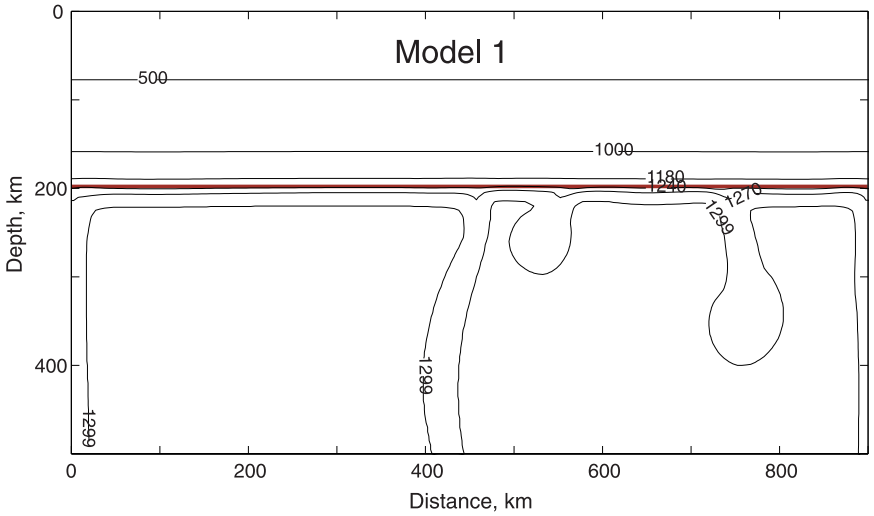

Figure 5. Potential temperature in degrees Celsius for model 1. This model is well into the rigid lid regime. The temperature contrast is small within downwellings. The thick red line shows the base of the rigid layer.

are instructive for fluid dynamics. However, they are not likely to be applicable to the modern Earth as stagnant lid heat flow from (11) is 62 mW m^{-2} and is larger than the heat flow in old ocean basins where a chemical lid does not exist. The temperature contrast at the base of the lid AT_η is 71 K. The temperature contrast within the downwellings is observable in the laboratory and potentially observable from tomography in the Earth. It is ~10 K in this model, much less than that the contrast at the base of the lid. The geotherms are essentially horizontal within the chemical layer.

3.2. Criteria for Chemical Lid to Stagnant Lid Transition

[27] We investigate the transition from convection beneath a rigid chemical lid to ordinary stagnant lid convection, which occurs as the normalized value of heat flow approaches 1 (Figure 2). In our models, this transition begins at a normalized boundary layer temperature contrast A of ~3 (Figure 4). However, the results for $A \geq 3$ show considerable scatter. Two normalized heat flow results with A = ~3.6 have the predicted value ~1 for a stagnant lid while two results for with A = ~4.5 have a normalized heat flow of ~0.9. The trend defined by points for $A \leq 3.6$ extrapolates to the predicted stagnant lid value at A = 4.5.

[28] We present a series of time-dependent models to further investigate the character of this transition, the character of which may be complex. We keep the temperature 1300°C at the base of the model stationary for simplicity. The initial condition is that the geotherm is linear from 0°C at the surface to the mantle adiabat at the base of the rigid layer and equal to the mantle adiabat below the rigid layer. Thus no rheological boundary layer initially exists beneath the lid, A = 0 and there is no convective heat flow beneath the lid. The normalized temperature contract across rheological boundary layer A increases as heat flows into the lid. We expect from (15) that A will increase with time so that the convective heat flow comes into steady state with conductive heat flow through the lid. In addition, we expect that the normalized heat flow will increase with A in the rigid lid mode but be independent of A in the stagnant lid mode.

[29] We begin with four models. Models 3 and 5 have T_η = 60 K, they differ slightly in viscosity, 0.9 × 10^{19} Pa s and 1.0 × 10^{19} Pa s, respectively. Models 2 and 4 share the viscosity of 1.3 × 10^{20} Pa s and T_η = 100 K. They differ in that the domain of calculation is 600 km deep by 1500 km wide in model 4, rather than 500 km by 900 km in the rest of the models.

[30] The evolution of the normalized heat flow and the normalized temperature contrast A is somewhat more complicated although all are in crude agreement with the trend of (21) (Figure 6). The normalized heat flow in Model 2 approaches the predicted stagnant lid value 1 while the heat flow in the other models in considerably below 1. Both models 2 and 4 show a kink-shaped transition at A = ~2.8, but models 3 and 5 do not.

[31] The artificial side boundary conditions do not have large effects, as the wide model 4 is similar to the narrow model 2. A more subtle effect may,

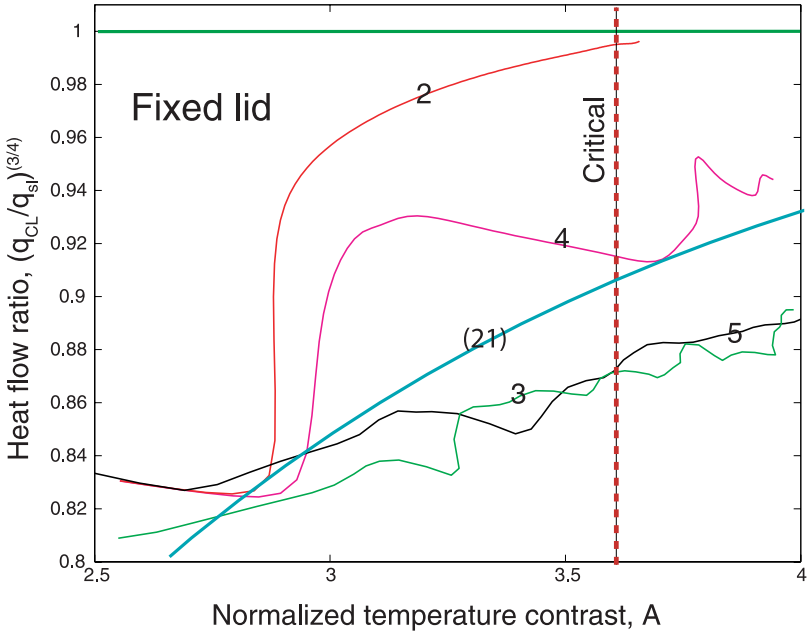

Figure 6. The evolution in time for four numerical models in the dimensionless coordinate system in scaling relationship (14). Model 2 approaches the stagnant lid limit. The others do not. We show the critical value of $A = 3.6$ for transition to stagnant lid behavior obtained below from additional models and the empirical curve (21) from Figure 4. The initial down-to-right slope of models 2 and 4 reflects the starting condition of a conducting lid extending to the base of the chemical layer. The heat flow in the lid at 177.5 km depth decreases by conduction as the temperature at the base of the chemical lid decreases and hence the temperature contrast below the lid increases. The heat flow increases once vigorous convection starts.

however, occur as a result of the geometry of the system. Model 2 organized so that there are downwellings at the sides and in the middle (Figure 7). The convection, though time dependent, approaches a steady state. Model 3 with the lower heat flow organized so that the central downwelling moved around (Figure 8). We do not attempt to find scaling relationships that capture the modest effect of the aspect ratio on flow wavelength.

[32] We computed another series of models that differ in viscosity from model 2 to quantify more

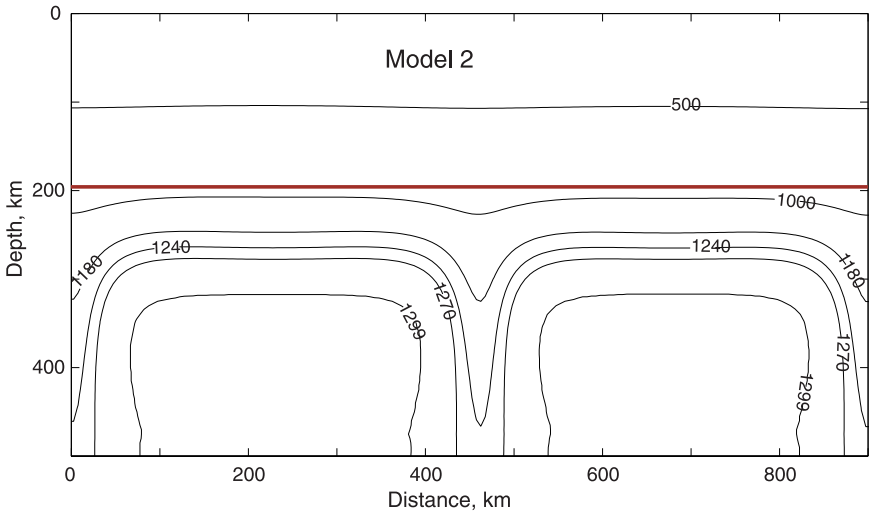

Figure 7. Potential temperature as in Figure 4 for model 2. The downwellings are at edges and center of the model. This model is just beyond the transition from rigid lid to stagnant lid. The thick red line shows the base of the rigid layer.

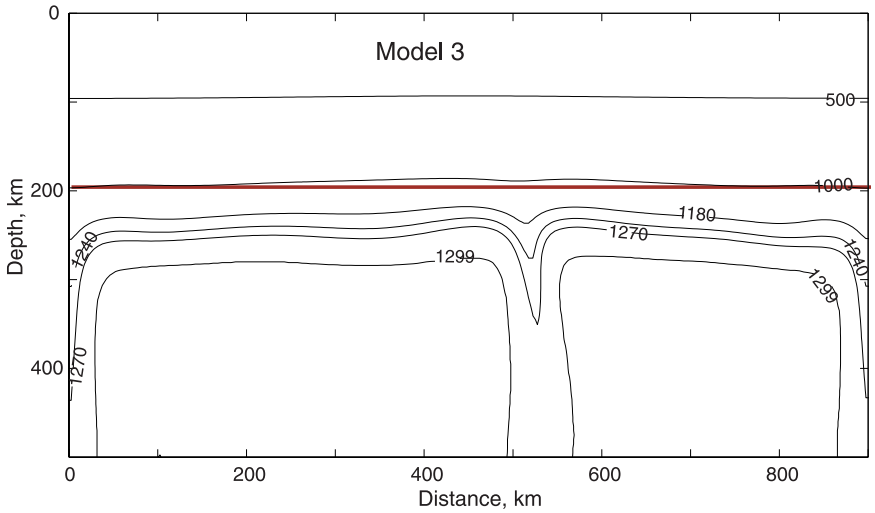

Figure 8. Potential temperature as in Figure 5 for model 3. The downwelling near center of the model moves around. This model is at the transition between rigid lid and stagnant lid. The thick red line shows the base of the rigid layer.

aspects of the transition from stagnant lid to rigid lid convection at long times where convective heat flow is in quasi-steady state with conduction through the chemical lid (Table 1).

[33] Model 2 is just within the stagnant lid regime. Keeping extra digits so that slight differences are evident, the predicted stagnant lid heat flow from (11) of model 2 is 14.218 mW m^{-2} (Table 1). The temperature at the base of the lid in equilibrium with this heat flow is $T_{SL} \equiv q_{SL} Z_{\rm lid}/k$, where $Z_{\rm lid}$ is the thickness of the conductive lid. At steady state, the laterally averaged temperature at the base of the lid is $T_C \equiv q_C Z_{\rm lid}/k$, where q_C is the laterally averaged heat flow. We use the computed heat flow after a long time (arbitrarily 2 B.Y.) and a shallow depth (arbitrarily 20-km) as appropriate stable long-term average value of q_C. The computed temperature contrast defined of model 2 is 363.59 K while the contrast implied by the predicted stagnant lid heat flow is 363.98 K. Heat flow at the base of the lid increases monotonically toward the stagnant lid value (Figure 9).

Table 1. Transition Model Parameters and Results[a]

Model	Viscosity (10^{20} Pa s)	Spinup Time (Ma)	Final Temperature Contrast (K)	Stagnant Lid Heat Flow (mW m^{-2})	Stagnant Lid Temperature Contrast (K)
2	1.3	240	363.59	14.218	363.98
6	1.2	210	359.63	14.602	338.70
7	1.1	200	368.26	15.032	310.39
8	1.0	190	362.26	15.517	278.46
9	0.9	170	350.11	16.072	241.93
10	0.8	160	345.68	16.715	199.60
11	0.7	140	344.62	17.476	149.50
12	0.6	130	330.21	18.397	88.86
13	0.5	110	311.78	19.550	12.96
14	0.4	90	291.83	21.060	negative
15	0.2	50	238.50	26.534	negative
16	0.1	25		33.430	negative

[a] The final temperature contrast between the base of the lid and the mantle adiabat is computed by extrapolating the linear geotherm from laterally average heat flow at 20 km depth and 2 B.Y to the base of the rigid lid, mathematically, $T_L - q\Delta\, Z_{\rm lid}/k$, where $\Delta Z_{\rm lid}$ is the thickness of the chemical lid. The stagnant lid contrast is the difference between the mantle adiabat and the temperature at the base of the lid assuming the stagnant lid heat flow, mathematically, $T_L - q_{SL}\, \Delta Z_{\rm lid}/k$. It is physically relevant in the stagnant lid regime and becomes negative when the stagnant lid heat flow is large. The models differ only in the assumed value of the viscosity of the underlying half-space.

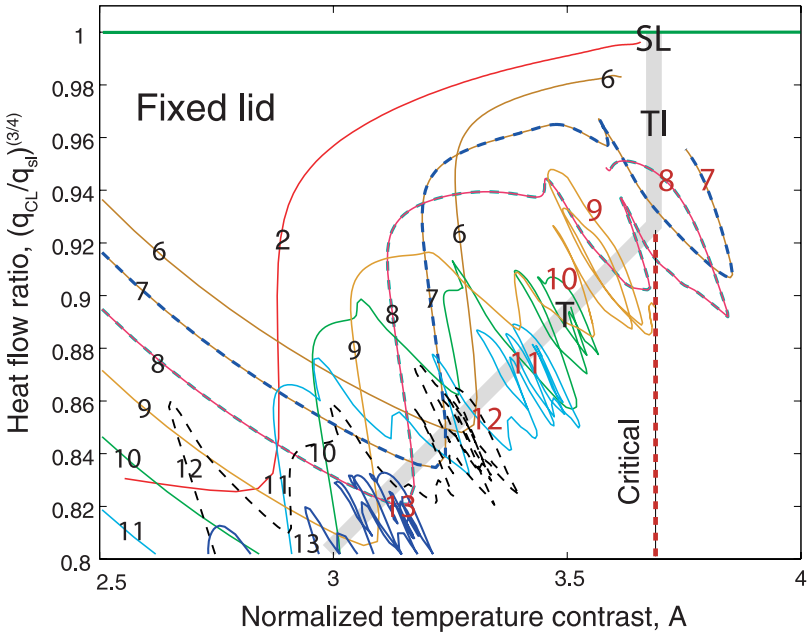

Figure 9. The evolution in time for numerical models in the dimensionless coordinate system in scaling relationship (14). These models differ from model 2 only in the half-space viscosity. The viscosity for models 2, 6, 7, 8, 9, 10, 11, 12, 13, 14, 15, and 16 is 1.3, 1.2, 1.1, 1.0, 0.9, 0.8, 0.7, 0.6, 0.5, 0.4, 0.2, and 0.1 $\times$ 10^{20} pa s, respectively. The thick gray line indicates domains: SL, stagnant lid; TI, transitional with heat flow independent of viscosity; and T, transitional to rigid lid. Models 14, 15, and 16 do not plot with the domain of the graph. The critical value of A for transition to stagnant lid behavior is ~3.6. The initial down-to-right slope of models 6–12 reflects the starting condition of a conducting lid extending to the base of the chemical layer. The heat flow in the lid at 177.5 km depth decreases by conduction as the temperature at the base of the chemical lid decreases and hence the temperature contrast below the lid increases. The heat flow increases once vigorous convection starts.

[34] Additional models also show that the critical normalized temperature contrast for transition between stagnant lid and rigid lid convection is ~3.6. The nature of the transition, however, is complicated in detail. We work from model 2 to models with progressively lower half-space viscosity η_0.

[35] Models with viscosities just below that of model 2 demarcate a parameter domain that is not evident from the scaling relationships. In particular, model 6 has a viscosity of 1.2 $\times$ 10^{20} Pa s. The heat flow at the base of the lid increases monotonically toward a limit that is less than the stagnant lid result (Figures 9 and 10). The temperature contrast beneath the lid from the heat flow at 25 km depth is 359.63 K.

[36] As the viscosity is decreased below that in the model 6, increasingly complicated time-dependent behavior is observed. The heat flow cycles diagonally on the graph between high temperature contrast with low normalized heat flow and low temperature contrast with high normalized heat flow. Moreover, the rising secular trend in the $(q_{CL}/q_{SL})^{3/4}$ with A results shifts to lower average values as the viscosity is reduced.

[37] The absolute heat flow, however, increases only slightly (Figure 10). The extrapolated average temperature contrast beneath the lid is 368.26 and 362.53 K for models 7 and 8. The computed contrast is resolvably less than 360 K, 350.11 K for model 9. Models 6, 7, and 8 thus define a regime where the long-term average rheological temperature contrast and the absolute long-term average heat flow are independent of the half-space viscosity and equal to that of the critical stagnant lid model 2. Another complicated behavior is that the temperature contrast in models 7 and 8 cycles into that of the stagnant lid regime >3.6 before returning to the lower values of chemical lid regime. Note further that the trend ends near model 7 with a normalized heat flow less than 1.

[38] Although the time-dependence of the transitional regime cannot be explained by our steady state theory, qualitative features of the limiting values of the secular trend in the data with A can

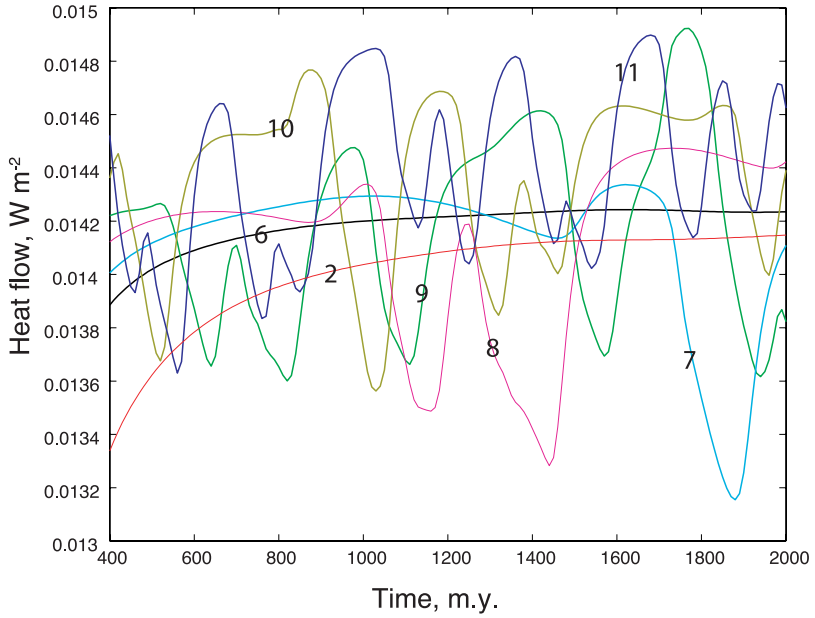

Figure 10. The computed laterally average heat flow for models in Table 1 as a function of time. Models 2 and 6 are monotonic. The other models oscillate. The viscosity for models 2, 6, 7, 8, 9, 10, and 11 is 1.3, 1.2, 1.1, 1.0, 0.9, 0.8, and 0.7×10^{20} Pa s, respectively.

be addressed. In particular, the weak sensitivity of the normalized heat flow to the temperature contrast A as A becomes smaller and ultimately approaches and becomes less than a (i.e., as the stagnant lid limit is approached) is expected from our derivation. To satisfy (7), the normalized temperature contrast will approach asymptotically a value at which the heat flow across the rheological sublayer is maximized. Indeed, from examination of (10) the steady state heat flow is a smooth function of the form $a_1^{2(n+1)} \exp(-a_1)$ of the temperature contrast across the rheological boundary layer. Heat flow is thus a weak function of the contrast (a_1 or A) near its maximum. The convection organizes with a contrast near the maximum but not to its precise value.

[39] Models 9, 10, 11, and 12 define another transitional regime where the normalized rheological temperature contrast remains below the critical value of ~3.6. The models become increasing time-dependent with decreasing half-space viscosity (Figures 10 and 11). Conduction through the rigid lid apparently limits the variation of heat flow. For example, changing the temperature at the base of the rigid lid by 50 K changes the heat flow by only 0.76 mW m^{-2}.

[40] Equation (12) provides a qualitative explanation for this cyclic behavior. The heat flow through the conductive lid adjusts slowly to the heat supplied by the underlying convection. High convective heat flow increases the temperature at the base of the lid, which decreases the normalized temperature contrast A. This, in turn, decreases the convective heat flow and the base of the lid cools leading to an increase in the temperature contrast available to drive convection. The flow is consequently more vigorous.

[41] Alternatively, the time dependence may be explained in terms of the growth and detachment of the gravitationally unstable rheological boundary layer in drips, which govern the heat flux from the cold boundary. Assuming a linear rheology (n = 1) and that the flow is in the stagnant lid regime the average $\Delta Z_{rheo} \propto Ra_{eff}^{-1/3}$ [*Davaille and Jaupart*, 1993a, 1993b] and the period of drip formation in the rheological boundary layer will scale as $\eta_o^{2/3}$ (cf. equation (A5)). Further examination of equations (15) and (21) and the foregoing results suggests that a comparable scaling exists for chemical lid convection. Thus, the time-dependence (including the time for the onset of convection) is expected to generally shift to shorter periods as the background viscosity declines, which is apparent in Figures 10 and 11. The startup time with a rigid chemical lid varies as $\eta_0^{7/9}$ in the models (Figure 12). See Appendix A for more discussion. A full analysis of the boundary layer dynamics of this transitional regime is of interest but beyond the scope of this paper.

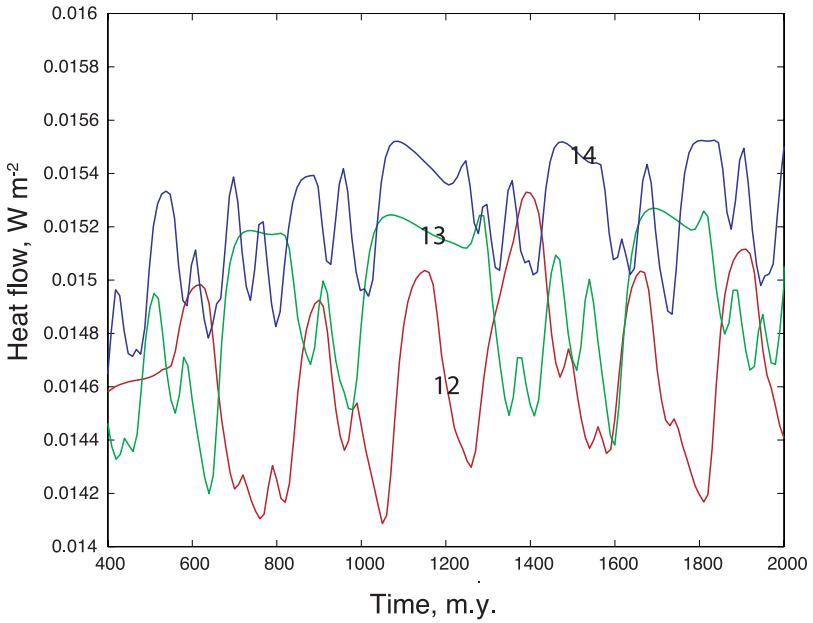

Figure 11. Computed heat flow histories for models in Table 1 as in Figure 10. These models have low viscosity and are in the rigid lid regime. The viscosity for models 12, 13, and 14 is 0.6, 0.5, and 0.4 $\times$ 10^{20} pa s, respectively.

3.3. Implications for Cratonal Thermal Structure

[42] The heat flow through the cratonal lithosphere and the temperature contrast at the base of the chemically buoyant layer are potentially observable from xenolith geotherms and seismic data. Overall our models capture the predictable part of the evolution of these parameters. The models are hence useful for examining the behavior of cratonal lithosphere over time and its current thermal structure. However, our work indicates that some unpredictability remains even if the relevant material properties are known. We thus include a caveat.

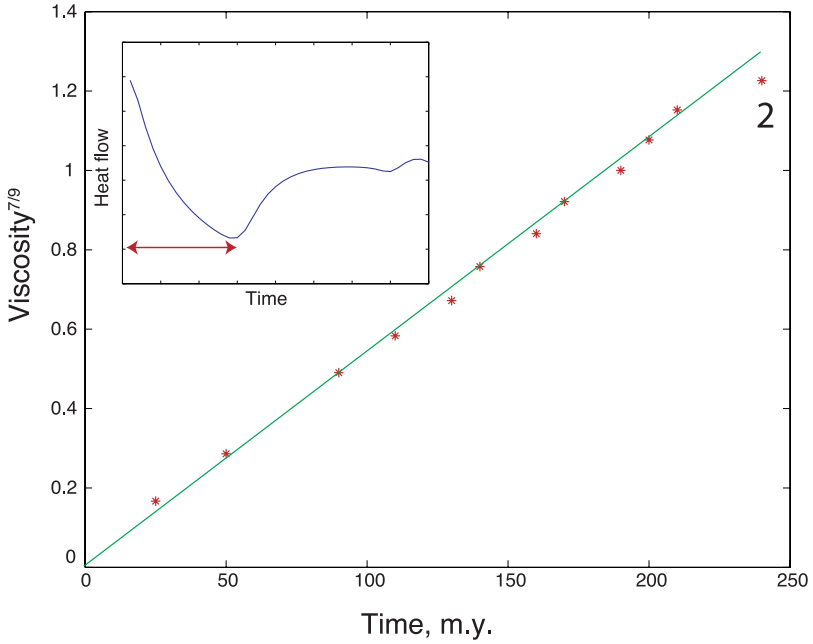

Figure 12. The half-space viscosity (in 10^{20} Pa s) to the 7/9 power as a function of startup time to reach the minimum in heat flow (inset) for models in Table 1. Model 2, which is in the stagnant lid regime, lies below the eyeball line defined by the other points.

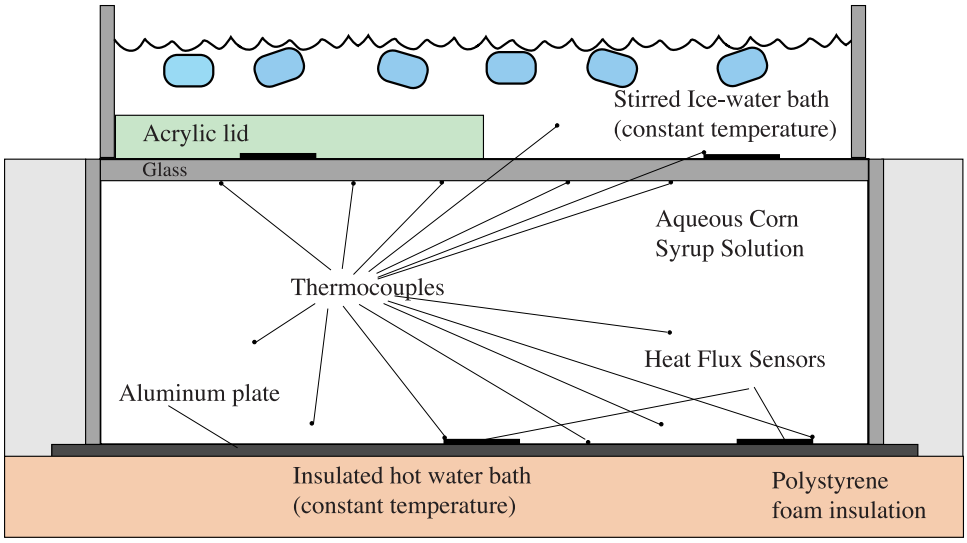

Figure 13. Schematic diagram of the experimental setup. The base of the lid is flat and the fluid is heated from below.

[43] First the computed heat flow oscillates in Figure 9 and the computed heat flow in Figure 4 show scatter. Some of the scatter involves the effects of artificial lateral boundaries that crudely represent the real finite extent of cratons. We also note that our assumption of steady state is not fully applicable. The heat flow in models in Figure 9, 10, and 11 evolved over a scale of 2 billion years, comparable to the timescale for secular cooling of the mantle. Numerous transient events would affect the base of real continental lithosphere over this time interval including the impingement of mantle plumes and the disruption of the orientation of convective rolls by changes in plate motion. For reference, plate motions reorganize on a time scale comparable to the age of the oldest ocean crust ~175 Ma [*Richards et al.*, 2000].

4. Some Laboratory Data

[44] Our representation of cratons as sites of chemical lid convection above a half-space is clearly an approximation. Cratons rest within moving plates and have finite width. It is thus relevant to see how robust our results are for cases where our assumptions are not strictly applicable. In particular, an example where our relationships fail provides caveats.

[45] We were unable to perform laboratory experiments directly representing quasi-steady convection beneath a chemical lid in a regime that is demonstrably transitional between the stagnant lid and isoviscous limits. That is, we do not have results for a continuous lid where the rheological temperature contrast A is small enough to be in the chemical lid regime but large enough to be away from the isoviscous limit. The main difficulty is that the region of the tank underlying the rheological boundary layer must be thick enough to behave like an isothermal half-space.

[46] A subset of new results from Jellinek and Lenardic (submitted manuscript, 2008) for convection heated from below for a continuous lid and a partial lid are relevant to test the robustness and general applicability of our theory to stagnant lid convection in the presence of a rigid chemical lid. In the work of Jellinek and Lenardic (submitted manuscript, 2008) convection is heated from below and cooled from above by constant temperature baths (Figure 13). At the cold boundary a thin glass plate separated the bath from the underlying fluid. To simulate the effects of a partial or complete chemical lid a Plexiglas sheet covering all or part of the glass is applied to form a rigid conducting lid. The geometry is obviously different from cratonal lithosphere, which hangs downward into the convecting regions. Thus, buoyant hot upwelling material does not get trapped by thin lithosphere beneath cratons as happens with plumes on the Earth. In addition, the heat flow through the lid is less than the heat flow through the gap. That is, the model cannot evolve to the same stagnant lid state beneath both lid and gap. Table 2 lists the physical properties of the convecting syrup and the setup.

Table 2. Experimental Properties

Property	Value
Glass thickness, m	0.005
Plexiglas thickness, m	0.012
Syrup layer depth, m	0.075
Conductivity glass, W m^{-1} K^{-1}	0.81
Conductivity Plexiglas, W m^{-1} K^{-1}	0.21
Conductivity syrup, W m^{-1} K^{-1}	0.365
Specific heat glass, J kg^{-1} K^{-1}	830
Specific heat Plexiglas, J kg^{-1} K^{-1}	1465
Specific heat syrup, J kg^{-1} K^{-1}	2616
Density glass, kg m^{-3}	2500
Density Plexiglas, kg m^{-3}	1180
Density syrup at average internal temp (50°C), kg m^{-3}	1395
Thermal diffusivity glass, m^2 s^{-1}	3.90E-07
Thermal diffusivity Plexiglas, m^2 s^{-1}	1.21E-07
Thermal diffusivity syrup, m^2 s^{-1}	1.00E-07
Thermal expansion coefficient syrup, K^{-1}	5.61E-04
$1/T_\eta$ syrup, K^{-1}	0.2 ± 0.2

[47] In the absence of a Plexiglas lid, the rheological temperature contrast beneath the complete lid was 5.54, which is well into the expected stagnant lid regime. The normalized heat flow q/q_{SL} from (11) is 1.045. This prediction is modestly dependent on viscosity. For example, a 8% error in viscosity equivalent to the 0.4 K uncertainty in interior temperature would cause a 3% change in the normalized heat flow. The prediction, however, is sensitive to the temperature scale T_η. For example, the 10% uncertainty in this parameter would change the predicted heat flow and the normalized ratio by 14%. Thus, the heat flow from the full lid experiment agrees with the stagnant lid prediction within the uncertainty of the physical parameters.

[48] The partial lid experiments are attractive in that convection self-organized so that there is a temperature gradient across the bottom boundary layer, a relatively isothermal interior, and there are temperature gradients across the upper boundary layers. The isothermal region underlies both the lid and the gaps; and thus avoids the difficulties in not knowing convection parameters. Specifically, the interior temperature, the interior viscosity, and the rheological temperature scale are the same beneath the conducting lid and the gap where only glass is present. It also allows the lid and gaps to approach quasi-steady state.

[49] We estimate the ratio q/q_{Sl} directly from the experiments as the ratio of the heat flow beneath the lid to that within the gap. This requires no knowledge of material parameters. We measure the temperature contrast beneath the lid and divide it by T_η to obtain the normalized temperature contrast A. The uncertainty in T_η similarly affects all the data points by ∼10%.

[50] Jellinek and Lenardic (submitted manuscript, 2008) reported experiments for lids covering 20, 43, 60, and 83% of the box. Qualitative results are shown in Figure 14. They found that the internal temperature and heat flow is reasonably expressed as a weighted contribution of the lid and lid-free sides, depending on the extent of thermal mixing. We present results in Figure 4 (points L). The points plot in the expected quadrant of the plot but do not follow the predicted trend.

[51] Ideally, the lid regions and the gap regions should be wide enough that convection beneath the two regions does not strongly interact. That is, full cells and not just upwellings or downwellings need to form in both regions. However, this is not the case in all the experiments. We qualitatively discuss the results beginning with the experiment (L8) where the lid covered 83% of the tank (Figure 14). Then, a strong downwelling occurred beneath the gap lowering its heat flow and a strong basal upwelling occurred at the boundary between the gap and the lid. The downwelling decreased heat flow in the gap and increased the ratio of lid heat flow to gap heat flow. At the other end, a strong basal upwelling occurred beneath the lid in experiment L2 where the lid covered 20% of the tank. This point and experiments L4 and L6 define a trend with a relatively constant heat flow ratio and increasing temperature contrast with decreasing lid coverage. The trend crosses the expected curve at the intermediate coverage of ∼43%.

[52] We note that although convection modulated by the gap-lid boundary occurred in experiment L4 independent stagnant lid and rigid cells did form over gap and lid, respectively. The point from this experiment falls near our numerically determined curve in Figure 3. This experiment thus gives limited support to the conclusions drawn from the numerical models.

[53] We conclude that that our theory did not adequately represent this attractive experimental arrangement when the gap-lid boundary or the lid localized strong basal upwellings. With regard to the Earth, the breadth of lid and gap regions needs to be large enough that convection cells beneath the regions do not strongly interact as occurred in

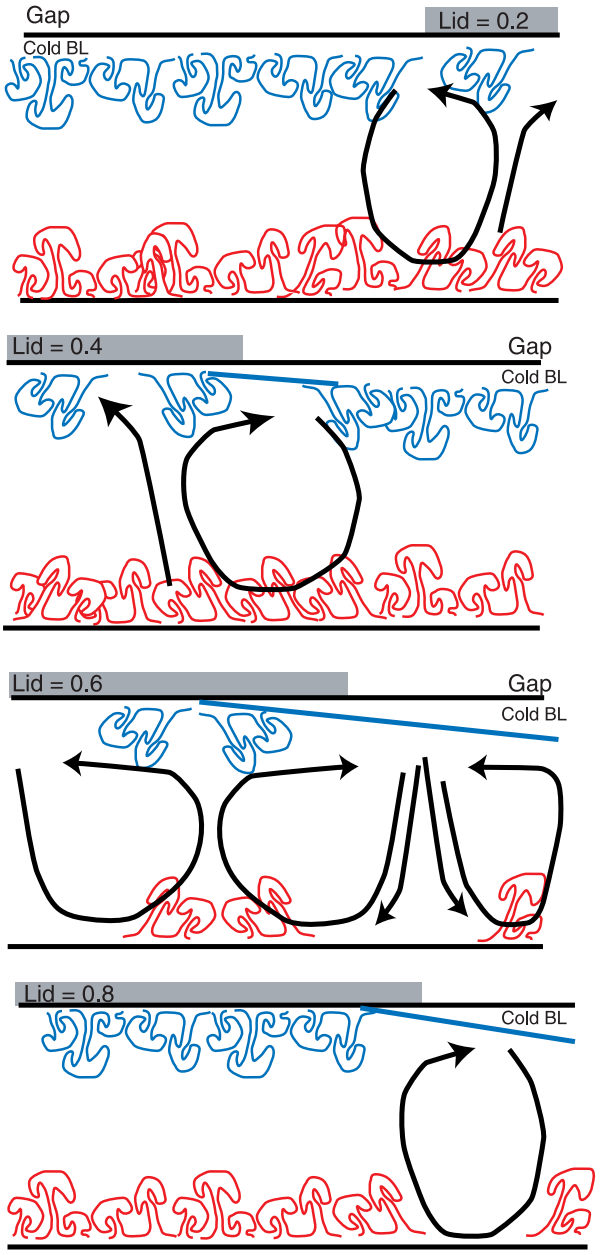

Figure 14. Platform of convection for partial lid experiments by Jellenik and Lenardic (submitted manuscript, 2008). Convection in the second panel where the lid covered 43% of the fluid organized into weakly interacting regions beneath the lid and the gap. The flow beneath lid and gap strongly interacted in the other experiments as illustrated. See text.

experiment L4. Cratons, platforms, and oceans are wide enough that this is not likely to be an issue.

5. Application to Freeboard

[54] The elevation of much of the area of continents and cratons is within a few hundred meters of sea level. Geologists use the term "freeboard" to describe the systematic variation of this elevation difference through geological time. This nautical term refers to the height of the deck of a ship above the water line. Continental freeboard has varied over the last 600 Ma. At times, shallow seas transgressed over the continents depositing marine sediments. At other times, the sea regressed exposing dry land. The general inference from the depth of erosion and the thickness of deposited sediments is that freeboard has not changed greatly (less than ~1 km) since cratons stabilized at ~2.5 Ga [e.g., *Galer and Mezger*, 1998].

[55] We discuss the effect of thermal structure on the behavior of freeboard in craton and platforms over the last several hundred million years where good geological records exist. Nonbuoyant lithosphere beneath platforms thickened significantly as the Earth's interior cooled monotonically over time, while the cratonal lithosphere did not cool much by comparison [*Sleep*, 2005]. To quantify this effect seen in Figure 1, we represent platform regions that lack chemically buoyant lithosphere with isochemical stagnant lid convection and cratons with chemical lid convection. Our parameterization then provides predictions for the variation of freeboard of cratons underlain by buoyant lithosphere relative to platforms underlain by normal mantle. It also provides the change of cratonal freeboard relative to ridge axes over time. This application utilizes predictable quantities from our scaling relationships. That is, we seek to explain the observation that sediments typically cover platform crust while Archean crust is typically bare.

5.1. Computation of Freeboard

[56] We develop a simple model for freeboard. For simplicity, we ignore radioactive heat generation and let thermal conductivity be constant. The geotherm beneath platforms is then linear down to the top of the rheological boundary layer. That is, the temperature is 0°C at the surface and the mantle adiabat minus the rheological temperature contrast ($T_L - a_1 T_\eta$) at the top of the rheological layer.

[57] A simple model for the rheological boundary layer assumes that the laterally averaged conductive heat flow decreases linearly with depth

$$q = q_c \left[\frac{z_B - s}{z_B} \right], \tag{22}$$

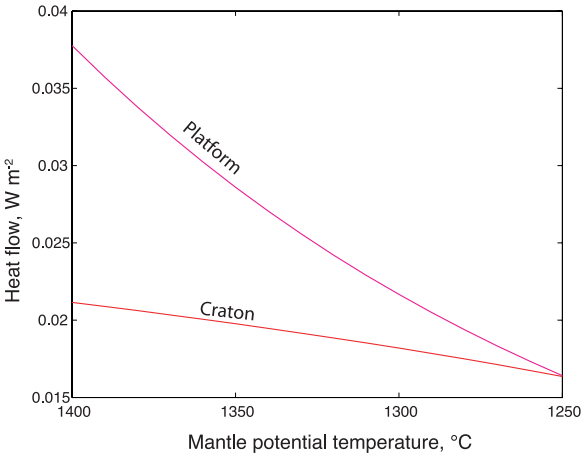

Figure 15. Computed heat flow through craton and platform lithosphere as a function of mantle potential temperature. These regions on the Earth evolve to the right as the Earth's interior cools.

where q_c is the conductive heat flow through the stagnant lid and s is the depth below the top of the rheological boundary layer and the depth scale

$$z_B = \frac{2ka_1T_\eta}{q_c}. \tag{23}$$

This implies that the thermal gradient in the rheological boundary layer is on average (over depth) about half the conductive gradient in the lid [*Sleep*, 2006]. With consideration of the volumetric thermal contraction an any time, the (negative) freeboard of platforms relative to the mantle adiabat is [*Sleep*, 2005]

$$F_P \approx \frac{\alpha k}{q_c}\left[\frac{T_L^2}{2} + \frac{a_1^2T_\eta^2}{6}\right]. \tag{24}$$

This elevation is also the thermal contribution to freeboard of the platform relative to the ridge axis. The first term in the brackets gives the freeboard that assuming that the thermal gradient extrapolates linearly to the mantle adiabat. The second term represents the effect of the finite temperature contrast across the rheological boundary layer. It is small compared to the leading term.

[58] The geotherm beneath the chemical lid is similar. The temperature is $T_L - AT_\eta$ at the base of the chemical lid at depth L. The geothermal gradient within the rheological boundary layer decreases with depth replacing a_1 in (24) with A. The negative freeboard of the craton is

$$F_C = \alpha\left[\frac{(T_L + AT_\eta)L}{2} + \frac{2kA^2T_\eta^2}{3q_c}\right], \tag{25}$$

where the conductive heat flow through the lid is

$$q_c = \frac{k(T_L - A)}{L}. \tag{26}$$

We numerically solve this equation and the scaling result in (21) to temperature contrast A to obtain the heat flow.

5.2. Freeboard Example

[59] We present as an example a one-dimensional model of freeboard with parameters calibrated for relevance to the modern Earth. The present mantle adiabat is 1300°C, T_η is 60 K, the chemical lid is 180 km thick, and the present stagnant lid heat flow is 1300 K times conductivity of 3 W m^{-1} K^{-1} divided by 180 km or 21.17 mW m^{-2}. We use a_1 = 2.4 from (7) for stagnant lid convection, as we are interested here in the depth where the geotherm approaches the conductive gradient.

[60] We take A = 3.6 and plot the heat flow as a function of potential temperature in Figure 15. The cratonal and platform heat flows converge when the temperature is $\leq$1250°C, indicating that the flow in both regions is governed by stagnant lid convection. Similarly, the cratonal and platform freeboard is identical at $\leq$1250°C (Figure 16). In the example, the free broad of platforms declined over about a 1 Ga evolution by a factor of 2 while the freeboard of cratons relative to ridges axes changed only slightly.

[61] Behavior during the last 500 Ma is relevant to continental geology. Platforms systematically subside relative to cratons independent of the details of the model and its assumptions. The rate of change of cratonal freeboard and platform freeboard at the present mantle temperature 1300°C is about 12.5 m K^{-1}. It is a weak function of potential temperature and hence time.

[62] The cooling rate of the mantle is not well constrained, but 50 K/B.Y. is a reasonable estimate [*Abbott et al.*, 1994; *Galer and Mezger*, 1998]. The ~25 K of cooling last 500 Ma implies that platforms subsided ~300 m relative to cratons. This rate is enough to explain why cratons stand higher than platforms [*Sleep*, 2005]. The load of sediments amplifies subsidence by a factor of 4 to 5. The kilometer or more of subsidence beneath sediments explains platform deposits but not thick basins like Michigan and Williston that are likely to be associated with the

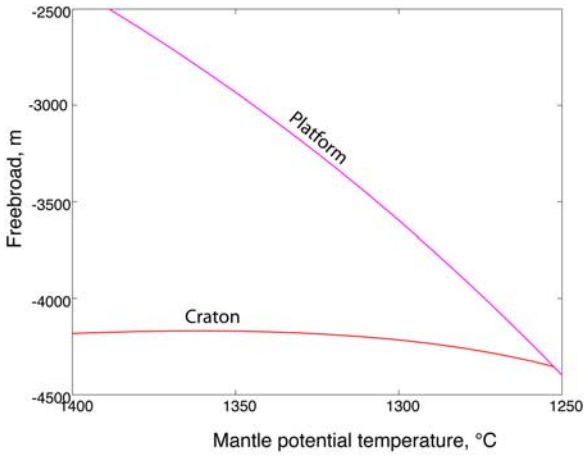

Figure 16. Thermal freeboard relative to the ridge axis of cratonal and platform lithosphere as a function of mantle temperature. The rate of convergence of the curves is the rate at which platforms subside relative to cratons.

cooling of lithosphere that was initially much thinner than its equilibrium value (Figure 1).

6. Conclusions

[63] Highly viscous, chemically buoyant cratonal lithosphere provides a conducting lid for the underlying convection. We represented this situation as convection beneath a rigid conducting lid over an adiabatic half-space in numerical and analytical models. We obtained dimensional scaling relationships in analogy with stagnant lid convection using the temperature T_η to change viscosity by a factor of e to normalize the temperature contrast being the base of lid and the adiabatic half-space. The convective heat flow scales to this normalized temperature to the 4/3 power when this quantity is less than 2.5. When the normalized temperature contrast is greater than ~3.6, the chemical lid has little affect on convection. We do not have a precise parameterization for the transition between normalized temperature contrasts of 2.5 and 3.6.

[64] We apply our parameterized convection formulation to the thermal history of cratonal and platform lithosphere underlain by stagnant lid convection. Platform lithosphere has thickened has the Earth's interior has cooled and become more viscous. Our computed differential subsidence between of platforms relative to cratons is 300 m in the last 500 Ma. This is sufficient to explain the tendency for cratons to outcrop and sediments to cover platforms.

Appendix A: Startup Time for Rigid Chemical Lid Convection

[65] The models shown in Figure 12 were started form a conductive geotherm intersecting the mantle adiabat at the base of the lid (Figure A1). We use (6) to extend the work of *Choblet and Sotin* [2000] and *Sleep* [2002] to cover this case.

[66] The minimum heat flow in Figure 12 occurs at a time where the convecting heat flow in the

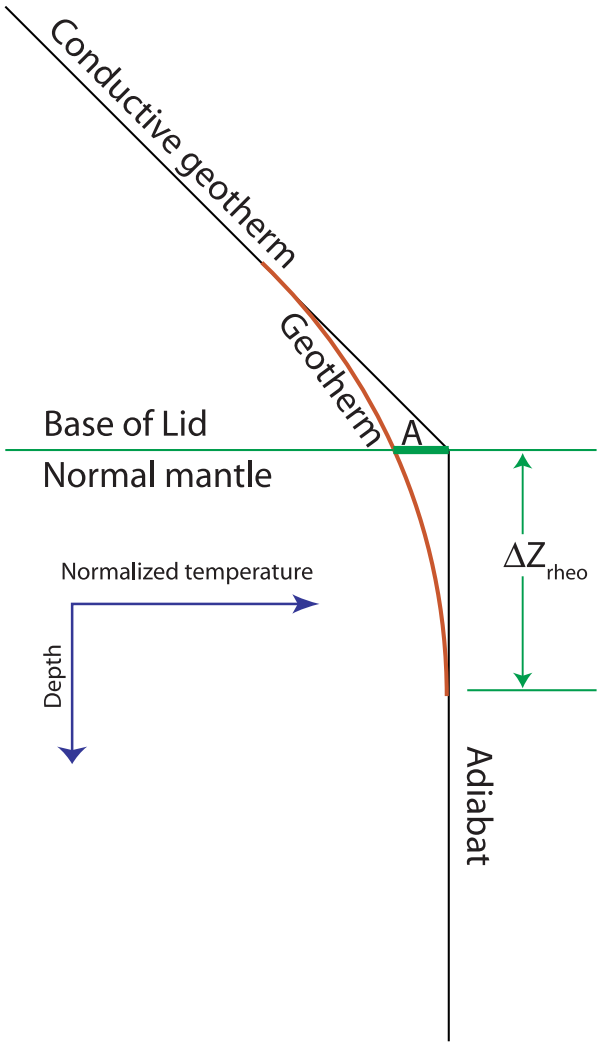

Figure A1. Schematic diagram for the starting geotherm in the models in Figure 12. The normalized temperature contrast A and the thickness of the rheological boundary layer ΔZ_{rheo} scale to the square root of time when conduction dominates over convection.

rheological boundary layer is a significant fraction of the heat flow convected through the lid, which is

$$q_L = \frac{k\left(T_L - AT_\eta\right)}{Z_{\text{lid}}}. \tag{A1}$$

This quantity does not vary a lot in the models in Figure 12 and Table 1 as $AT_\eta \ll T_L$. We keep treat q_L as a constant to obtain simple expressions for the startup time where convective heat flow scales with this quantity.

[67] Initially, convection is weak and the geotherm is essentially that due to conduction. Both the normalized temperature contrast A and the thickness of the rheological boundary layer ΔZ_{rheo} increase with the square root of time (Figure A1). We assume that they are less than their final values in equilibrium with stagnant lid convection, that is, $A < a_1$. We cannot, however, ignore the exponential term in (6). Equation (6) for a linear viscosity $n = 1$ then applies beneath the lid. Replacing the scaling parameter a_1 with the normalized temperature contrast A dimensionally yields

$$q_L \approx \frac{\rho C A^2 T_\eta^2 \rho g \alpha \Delta Z_{\text{rheo}}^2}{\eta_0 \exp(A)}. \tag{A2}$$

The normalized temperature contrast is proportional to the thickness of the rheological boundary layer in this case,

$$A \approx \frac{q_L \Delta Z_{\text{rheo}}}{kT_\eta}. \tag{A3}$$

Combining (A2) and (A3) yields

$$q_L \approx \frac{\rho C q_L^2 \rho g \alpha \Delta Z_{\text{rheo}}^4}{k^2 \eta_0 \exp(A)}, \tag{A4}$$

which is independent of the rheological temperature scale T_η. The time for conduction to diffuse heat over the depth range ΔZ_{rheo} is dimensionally

$$t_L = \Delta Z_{\text{rheo}}^2 / \kappa. \tag{A5}$$

Combining (A4) and (A5) yields

$$q_L = \left[\frac{q_L^2 \rho g \alpha}{\rho C \eta_0 \exp(A)}\right] t_L^2. \tag{A6}$$

The starting conductive heat flow q_L is constant in the models in Figure 12. Only the half-space viscosity η_0 was varied. This case yields the relevant proportionality for startup time

$$t_L \propto \eta_0^{1/2} \exp(A/2) \approx \eta_0^{7/9}, \tag{A7}$$

where the second approximate equality is the eyeball line in Figure 12. Note the startup time in (A7) depends on viscosity more strongly on half-space viscosity than the 1/2 power. The normalized temperature contrast across the rheological boundary layer A in (A7) is implicitly a function that increases with half-space viscosity (Table 1).

Acknowledgments

[68] This research was in part supported by NSF grant EAR-0406658. AMJ acknowledges support from the Canadian Institute for Advanced Research and from the NSERC. We thank Sarah Wait Zaranek and Michael Manga for attempting physical experiments. Two anonymous reviewers and associate editor Magali Billen provided helpful comments.

References

Abbott, D. L., L. Burgess, J. Longhi, and W. H. F. Smith (1994), An empirical thermal history of the Earth's upper mantle, *J. Geophys. Res.*, *99*, 13,835–13,850, doi:10.1029/94JB00112.

Bell, D. R., M. D. Schmitz, and P. E. Janney (2003), Mesozoic thermal evolution of the southern African mantle lithosphere, *Lithos*, *71*, 273–287, doi:10.1016/S0024-4937(03)00117-8.

Carlson, R. W., and R. O. Moore (2004), Age of the Eastern Kaapvaal mantle: Re-Os isotope data for peridotite xenoliths from the Monastery kimberlite, *S. Afr. J. Geol.*, *107*, 81–90, doi:10.2113/107.1-2.81.

Choblet, G., and C. Sotin (2000), 3D thermal convection with variable viscosity: Can transient cooling be described by a quasi-static scaling law, *Phys Earth Planet Inter*, *119*, 321–336, doi:10.1016/S0031-9201(00)00136-9.

Chulick, G. S., and W. D. Mooney (2002), Seismic structure of the crust and uppermost mantle of North America and adjacent oceanic basins: A synthesis, *Bull. Seismol. Soc. Am.*, *92*, 2478–2492.

Cottrell, E., C. Jaupart, and P. Molnar (2004), Marginal stability of thick continental lithosphere, *Geophys. Res. Lett.*, *31*, L18612, doi:10.1029/2004GL020332.

Davaille, A., and C. Jaupart (1993a), Thermal convection in lava lakes, *Geophys. Res. Lett.*, *20*, 1827–1830, doi:10.1029/93GL02008.

Davaille, A., and C. Jaupart (1993b), Transient high-Rayleigh-number thermal convection with large viscosity variations, *J. Fluid Mech.*, *253*, 141–166, doi:10.1017/S0022112093001740.

Davaille, A., and C. Jaupart (1994), The onset of thermal convection in fluids with temperature-dependent viscosity: Application to the oceanic mantle, *J. Geophys. Res.*, *99*, 19,853–19,866, doi:10.1029/94JB01405.

Galer, S. J. G., and K. Mezger (1998), Metamorphism denudation and sea level in the Archean and cooling of the Earth, *Precambrian Res.*, *92*, 389–412, doi:10.1016/S0301-9268(98)00083-7.

Griffin, W. L., S. Y. O'Reilly, L. M. Natapov, and C. G. Ryan (2003a), The evolution of the lithospheric mantle beneath the Kalahari Craton and its margins, *Lithos*, *71*, 215–241, doi:10.1016/j.lithos.2003.07.006.

Griffin, W. L., S. Y. O'Reilly, N. Abe, S. Aulbach, R. M. Davies, N. J. Pearson, B. J. Doyle, and K. Kivi (2003b), The origin and evolution of Archean lithospheric mantle, *Precambrian Res.*, *127*, 19–41, doi:10.1016/S0301-9268(03)00180-3.

Jaupart, C., P. Molnar, and E. Cottrell (2007), Instability of a chemically dense layer heated from below and overlain by a deep less viscous fluid, *J. Fluid Mech.*, *572*, 433–469, doi:10.1017/S0022112006003521.

Kaminski, E., and C. Jaupart (2000), Lithospheric structure beneath the Phanerozoic intracratonal basins of North America, *Earth Planet. Sci. Lett.*, *178*, 139–149, doi:10.1016/S0012-821X(00)00067-4.

Lehtonen, M. L., H. E. O'Brien, P. Peltonen, B. S. Johanson, and L. K. Pakkanen (2004), Layered mantle at Karelian craton margin: P-T of mantle xenocryst and xenoliths from the Kaavi-Kuopio kimberlites, Finland, *Lithos*, *77*, 593–608, doi:10.1016/j.lithos.2004.04.026.

Lenardic, A., L. N. Moresi, A. M. Jellinek, and M. Manga (2005), Continental insulation, mantle cooling, and the surface area of oceans and continents, *Earth Planet. Sci. Lett.*, *234*, 317–333, doi:10.1016/j.epsl.2005.01.038.

Mooney, W. D., and J. E. Vidale (2003), Thermal and chemical variations in subcrustal cratonic lithosphere: Evidence from crustal isostasy, *Lithos*, *71*, 185–193, doi:10.1016/j.lithos.2003.07.004.

Richards, M. A., H.-P. Bunge, and C. Lithgow-Bertelloni (2000), Mantle convection and plate motion history, in *The History and Dynamics of Global Plate Motions*, *Geophys. Monogr. Ser.*, vol. 121, edited by M. A. Richards, R. G. Gordon, and R. D. van der Hilst, pp. 289–307, AGU, Washington, D. C.

Shapiro, S. S., B. H. Hager, and T. H. Jordan (1999a), The continental tectosphere and Earth's long-wavelength gravity field, *Lithos*, *48*, 135–152, doi:10.1016/S0024-4937(99)00027-4.

Shapiro, S. S., B. H. Hager, and T. H. Jordan (1999b), Stability and dynamics of the continental tectosphere, *Lithos*, *48*, 115–133, doi:10.1016/S0024-4937(99)00025-0.

Shirey, S. B., J. W. Harris, S. H. Richardson, M. Fouch, D. E. James, P. Cartigny, P. Deines, and F. Viljoen (2003), Regional patterns in the paragenesis and age of inclusion in diamond, diamond composition, and the lithospheric seismic structure of Southern Africa, *Lithos*, *71*, 243–258, doi:10.1016/j.lithos.2003.07.007.

Shirey, S. B., S. H. Richardson, and J. W. Harris (2004), Integrated models of diamond formation and craton evolution, *Lithos*, *77*, 923–944, doi:10.1016/j.lithos.2004.04.018.

Sleep, N. H. (2002), Local lithospheric relief associated with fracture zones and ponded plume material, *Geochem. Geophys. Geosyst.*, *3*(12), 8506, doi:10.1029/2002GC000376.

Sleep, N. H. (2003a), Survival of Archean cratonal lithosphere, *J. Geophys. Res.*, *108*(B6), 2302, doi:10.1029/2001JB000169.

Sleep, N. H. (2003b), Geodynamic implications of xenolith geotherms, *Geochem. Geophys. Geosyst.*, *4*(9), 1079, doi:10.1029/2003GC000511.

Sleep, N. H. (2005), Evolution of continental lithosphere, *Annu. Rev. Earth Planet. Sci.*, *33*, 369–393, doi:10.1146/annurev.earth.33.092203.122643.

Sleep, N. H. (2006), Mantle plumes from top to bottom, *Earth Sci. Rev.*, *77*(4), 231–271, doi:10.1016/j.earscirev.2006.03.007.

Sleep, N. H. (2007), *Plate Tectonics Through Time, Treatise on Geophys.*, vol. 9, edited by G. Schubert, pp. 101–117, Elsevier, Oxford, U. K.

Solomatov, V. S., and L.-N. Moresi (2000), Scaling of time-dependent stagnant lid convection: Application to small-scale convection on Earth and other terrestrial planets, *J. Geophys. Res.*, *105*, 21,795–21,817, doi:10.1029/2000JB900197.